Shake table tests of a steel-concrete composite rigid-frame bridge subjected to a surface fault rupture

Yuanzheng Lin[1], Zhouhong Zong[2], Hong Hao[3] and Kaiming Bi[4]

1. Corresponding Author. PhD student, School of Civil Engineering, Southeast University, Nanjing 211189, China; Centre for Infrastructure Monitoring and Protection, School of Civil and Mechanical Engineering, Curtin University, Bentley, WA 6102, Australia. Email: linyz@seu.edu.cn

2. Professor, School of Civil Engineering, Southeast University, Nanjing 211189, China. Email: zongzh@seu.edu.cn

3. John Curtin Distinguished Professor, Centre for Infrastructure Monitoring and Protection, School of Civil and Mechanical Engineering, Curtin University, Bentley, WA 6102, Australia. Email: hong.hao@curtin.edu.au

4. Senior Lecturer, Centre for Infrastructure Monitoring and Protection, School of Civil and Mechanical Engineering, Curtin University, Bentley, WA 6102, Australia. Email: kaiming.bi@curtin.edu.au

Abstract

In the past two decades, several earthquake reconnaissance reports have demonstrated that bridges are very vulnerable when subjected to surface fault ruptures, but the relevant studies are insufficient to interpret the influence of surface rupture, especially for thrust faults. It is therefore necessary to examine the performances of fault-crossing bridges and consider potential solutions to mitigate the structural damage induced by surface fault rupture. On the other hand, steel-concrete composite rigid-frame bridge (SCCRFB) with concrete-filled double skin steel tube (CFDST) piers is a recently proposed structural solution with improved seismic performance compared to the conventional prestressed concrete (PC) rigid-frame bridge, and has great potential to withstand the tectonic dislocation of a fault. To understand the seismic performance of the innovative SCCRFB subjected to the surface fault rupture, shake table tests of a 1:10 scaled three-span SCCRFB subjected to across-fault ground motions that simulate a thrust fault were performed. The test results and discussions are reported in this paper.

Keywords: SCCRFB; shake table test; fault-crossing; seismic response; seismic damage.

1. INTRODUCTION

Multi-span bridges may suffer significant damages when traversed by a surface fault rupture during an earthquake. The damages are mainly due to the combined effects of strong ground shaking and static fault displacement (Somerville 2002) as evidenced in many past earthquake events (Kawashima 2002). Recently, a new structural solution, the steel-concrete composite rigid-frame bridge (SCCRFB) with concrete-filled double skin steel tube (CFDST) piers, is proposed by the authors. Due to its special structural layout, this novel bridge type is believed has superior seismic performance and better ability to prevent collapse compared to conventional prestressed concrete (PC) rigid-frame bridges, and better ability to withstand extreme seismic loading from a surface fault rupture passing through the bridge.

In recent years, some research works have been carried out to understand the seismic behaviour of bridges crossing fault-rupture zones (Yang and Mavroeidis 2018). Previous studies revealed that compared to traditional uniform seismic excitations, bridges subjected to across-fault ground motions will exhibit significant quasi-static responses and torsional damages due to the different excitations and permanent ground displacements on the two sides of the fault (e.g. Saiidi et al. 2013). However, these studies mainly considered the strike-slip fault, which means two blocks of the fault move horizontally and slide past one another, while the dip-slip fault (namely, two blocks move obliquely with a dip angle) has not been well investigated. Moreover, current studies on this topic are primarily confined to theoretical analysis (Goel and Chopra 2009, Goel and Chopra 2009) and numerical simulation (Roussis et al. 2003, Ucak et al. 2014, Xu and Lin 2017), while large-scale shake table tests of fault-crossing bridges are relatively limited (Saiidi et al. 2013). To the best knowledge of the authors, no relevant test that considers a dip-slip thrust fault has been reported yet.

This paper presents shake table studies on the seismic behaviours of the innovative SCCRFB with CFDST piers subjected a dip-slip thrust fault. A 1:10 scaled three-span SCCRFB model was constructed and tested by using the two-shake table system at Chongqing Communications Research and Design Institute (CCRDI), China. The bridge design, test procedure and test results are presented.

2. BRIDGE MODEL DESIGN

The testing bridge model was a 1:10 scaled three-span SCCRFB with CFDST piers. Its detailed geometries and materials are presented in Fig. 1. The bridge model was in total 15.6 m long with the span arrangement of 4 m + 7 m + 4 m, and the total height was 3.88 m, including footing (thickness of 0.4 m), column (height of 3.0 m) and girder (height of 0.48 m) (see Fig. 1(a)). The bridge superstructure was a steel-concrete composite box girder made of an open-section U-shaped steel box girder, a RC deck with the dimension of 1200 mm × 80 mm (width × height) connected with stud shear connectors (Fig. 1(b)). The substructure of the bridge model included four piers with two different types. In particular, two conventional RC double-column piers were placed on the two sides (namely, Piers 1 and 4), and each of them supported the bridge girder through two bi-directional sliding bearings. Each column had a circular section with a diameter of 192 mm and was reinforced by 10 φ8 longitudinal steel bars and φ6 stirrups spacing at 60 mm (Fig. 1(c)). The two middle piers, i.e. Piers 2 and 3, were the rectangular CFDST columns with outer steel box dimension of 480 mm × 240 mm and inner steel box dimension of 320 mm × 120 mm (Fig. 1(d)), and they were connected with the bridge girder through rigid joints. The φ10 reinforcement bars were used in the footings, the bent caps, and the bridge decks. Details about the specimen dimensions

and material grades are given in Fig. 1. A material test was performed prior to the shake table tests and the key parameters for different materials are summarized in Table 1, where E is Young's modulus, f_y is the yield strength of the steel rebars, f_c' represents cubic compressive strength of concrete, and ρ stands for density.

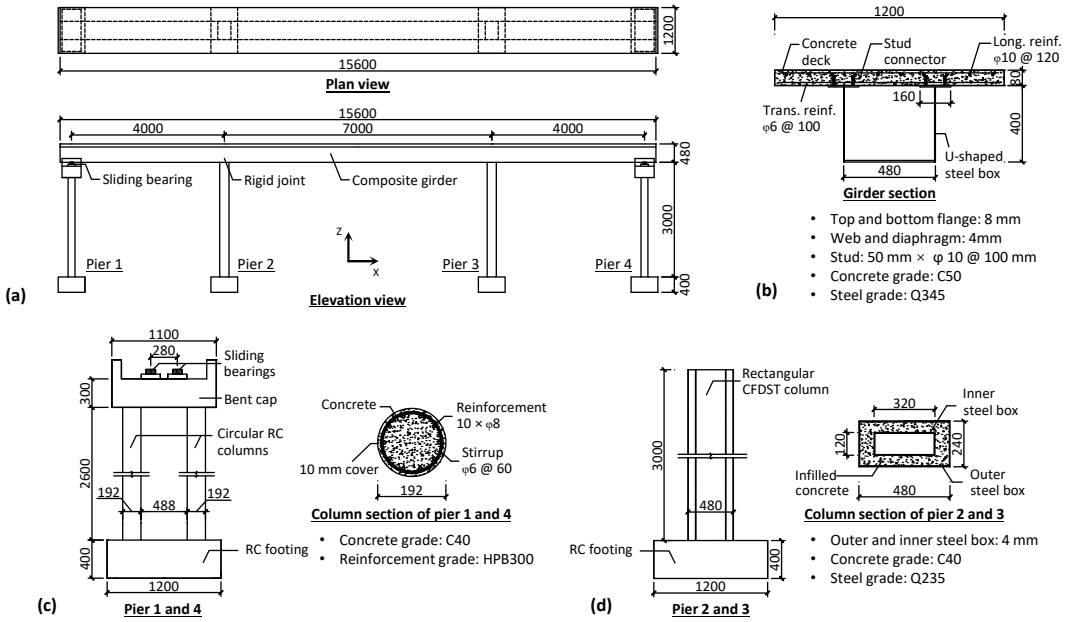

Fig. 1. Geometry and material details of the bridge model (unit: mm): (a) general view; (b) cross section of the bridge girder; (c) side piers; (d) middle piers

Table 1. Material properties

Material	Type	E (GPa)	f_y (MPa)	f_c' (MPa)	ρ (kg/m^3)
Steel plate	4 mm	210	320	-	7800
	8 mm	209	470	-	7800
Reinforcement	φ6	201	490	-	7800
	φ8	201	480	-	7800
Concrete	C40	31	-	40	2350
	C50	35	-	57	2250

3. TEST PROGRAM

The shake table system at CCRDI includes two tables. Each table has a size of 3 m × 6 m (transverse × longitudinal) and is able to carry a specimen with a maximum weight of 35 tonnes. The effective working frequency ranges from 0.1 Hz to 100 Hz. The two shake tables both have six degrees of freedom (DOFs) and can achieve a maximum acceleration of 1.0g in the three directions with full payload. The strokes are ±150 mm and ±100 mm in the horizontal and vertical directions, respectively.

The components of the bridge model were constructed separately and then assembled together to form the testing model. Fig. 2 shows the experimental setup. Because the bridge specimen was a scaled model, in total 21.86 tonnes of additional mass was installed onto the girder and piers to provide enough axial load and inertial forces for the bridge piers. The measuring instruments include 23 accelerometers, 7 displacement sensors, and 22 steel strain gauges, and they were installed on the key locations of the bridge model to record corresponding testing data. Because the testing bridge is a scaled model, relevant physical quantities should follow the similitude laws, and Table 2 summaries the basic similarity ratios in the test.

The ground motions recorded at the strong motion stations TCU049 and TCU052 in the 1999 Chi-Chi earthquake were used in the shake table tests. These two stations located very close to the surface rupture of Chelungpu fault but on different sides. The tectonic dislocation between the two stations during the mainshock was a typical thrust fault (Shin and Teng 2001), and this effect was intended to be simulated on the shake tables. To maximize the effect of dip-slip on the testing specimen, it is assumed that the bridge went across the fault rupture in the normal direction, i.e. the longitudinal (X) and transverse (Y) directions of the bridge are parallel to the fault-normal and fault-parallel directions respectively (see Fig. 2(b)), and the ground motions TCU049 and TCU052 were intended to be reproduced on Table A and Table B, respectively. In order to investigate the influence of pure dip-slip, the transverse components of the ground motions were not considered in the tests. The input ground motions were obtained based on the raw ground motion data after using a series of data processing procedures. In particular, a baseline correction technique to remove the baseline shifting errors (Lin et al. 2018) was applied, and the amplitudes of low-frequency portions were moderately scaled down to satisfy the stroke limitations of the actuators of the shake tables. Moreover, the time duration was compressed by a factor of 0.285 according to the scaling law as shown in Table 2. Fig. 3 shows acceleration and displacement time histories of the across-fault. It can be seen that the input ground motions were very different for the two shake tables. In particular, the differential displacement between the two tables was able to characterize the tectonic dislocation of a thrust fault.

In the tests, four different seismic intensities were considered, and the PGD was used as the control parameter to scale the input ground motions for each case. In particular, the component in the longitudinal direction of Table B was used as the controlling motion, and four different PGDs, namely -20 mm, -60 mm, -100 mm and -140 mm, were considered. The other components of the ground motions including those on Table A were accordingly scaled based on the PGD ratios of the reconstructed ground motions. The target peak ground accelerations (PGAs) and peak ground displacements (PGDs) for each case are listed in Table 3.

Table 2. Similarity ratios

Physical quantity	Similarity relationship	Value
Length (l)	S_l	0.1
Mass density (ρ)	S_ρ	8.1
Elastic modulus (E)	S_E	1
Mass (m)	$S_m = S_\rho S_l^3$	0.0081
Stiffness (k)	$S_k = S_E S_l$	0.1
Time (t)	$S_t = (S_m/S_k)^{0.5}$	0.285
Force (F)	$S_F = S_E S_l^2$	0.01

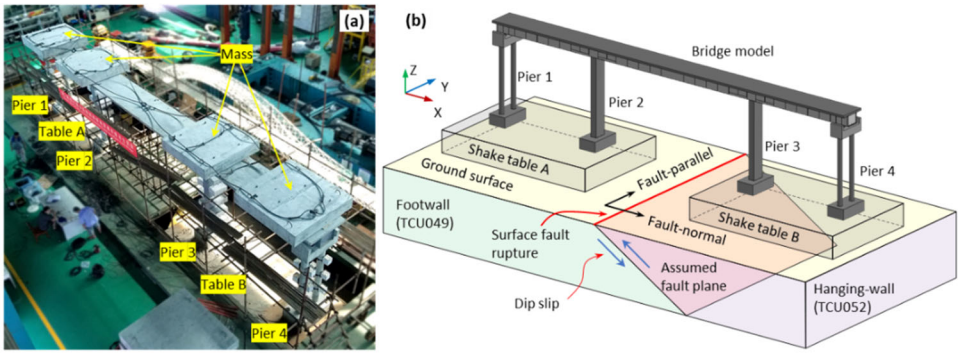

Fig. 2. Experimental setup: (a) general view; (b) positions of the bridge model and the assumed fault.

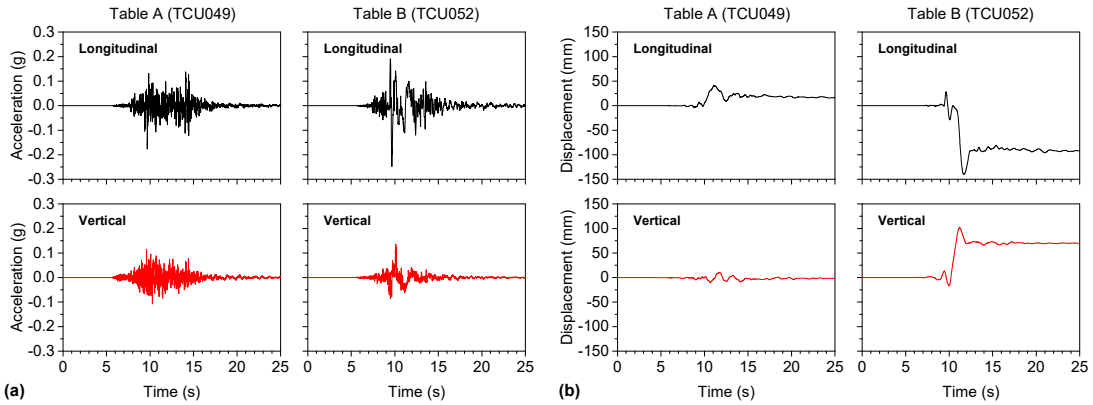

Fig. 3. Across-fault ground motions: (a) acceleration; (b) displacement.

Table 3. Test cases

Case	Direction	Table A		Table B	
		PGA (g)	PGD (mm)	PGA (g)	PGD (mm)
1	X	0.03	5.86	0.04	-20.00
	Z	0.02	1.55	0.02	14.54
2	X	0.08	17.59	0.12	-60.00
	Z	0.06	4.64	0.06	43.63
3	X	0.14	29.31	0.20	-100.00
	Z	0.10	7.74	0.10	72.71
4	X	0.20	41.04	0.29	-140.00
	Z	0.14	10.83	0.14	101.80

4. TEST RESULTS

The behaviour and damage of the bridge model were carefully checked after each test. For Cases 1 and 2, the structural vibrations and deformations were small because the seismic intensities were relatively small. When the input PGD increased to 100 mm (Case 3) and 140 mm (Case 4), structural deformations caused by the differential displacements of the two shake tables were clearly observed. Fig. 4 shows the deformations of the bridge model after Case 4. It can be seen that the right span of the bridge model was lifted up by shake table B through Pier 3, leading to the separation between the bridge girder and the bearings on Pier 4. It is also observed that Piers 2 and 3 tilted away from each other due to the longitudinal movement of the two tables.

The damages of the bridge model mainly located at the two ends of the middle piers. Fig. 5 shows the damages at the two middle piers after Case 4. As shown, local buckling occurred to the steel skins at the upper and lower ends of the two middle piers. After the tests, the steel skins around these areas were removed and it was found that the infilled concrete crushed at the bottom of the columns, and there were transverse cracks crossing the entire cross section of the two middle piers. It should be noted that some minor cracks also developed on the concrete surfaces of other members, while the strain data indicated that the steel plates and reinforcements of these members remained in the elastic range, which indicated that these damages were relatively insignificant compared to the middle piers.

Fig. 6 shows the bridge responses to the across-fault ground motions in the longitudinal direction in each case. It can be seen in Fig. 6(a) that the peak acceleration responses of the bridge girder were between the input PGAs on Table A and Table B as shown in

Table 3, and they increased almost linearly with the increase of the ground motion intensity. On the other hand, obvious quasi-static responses were obtained in the displacement time histories. As shown in Fig. 6(b), the bridge girder showed permanent displacements due to the differential permanent displacements on the two tables, while the dynamic responses (i.e. the fluctuations) were relatively small. The different fling-steps on the two tables also induced residual deformations in the four piers, and the drift responses were very different in the four cases as shown in Fig. 6(c). These results indicated that the bridge responses were dominated by the quasi-static deformation induced by fault dislocation.

Fig. 7 shows the peak and residual drift ratios of the four bridge piers in the longitudinal direction. It can be seen that the peak and residual drift ratios of the two middle piers increased almost linearly with the increase of seismic intensity, and the drift ratios of Pier 2 was larger than that of Pier 3, which might be due to the effect of vertical dislocation between the two tables. It is also noted that the drift ratios of Pier 4 were relatively small, and the reason is that Pier 4 separated with the bridge girder as shown in Fig. 4, which in turn released the horizontal force to Pier 4. The drift ratios of Pier 1 were close to that of Pier 2 when the PGD was not larger than 100 mm, however the sliding effect led to a decreasing trend when the PGD reached 140 mm (Case 4).

It should be noted that the bridge model only suffered minor damages at the top and bottom ends of the two middle piers during the tests though the maximum differential displacements in the longitudinal and vertical directions reached 170 mm and 103 mm respectively, which demonstrates the good seismic resistance capability of this type of bridge. It has great application potentials especially when they are constructed near or above an active fault.

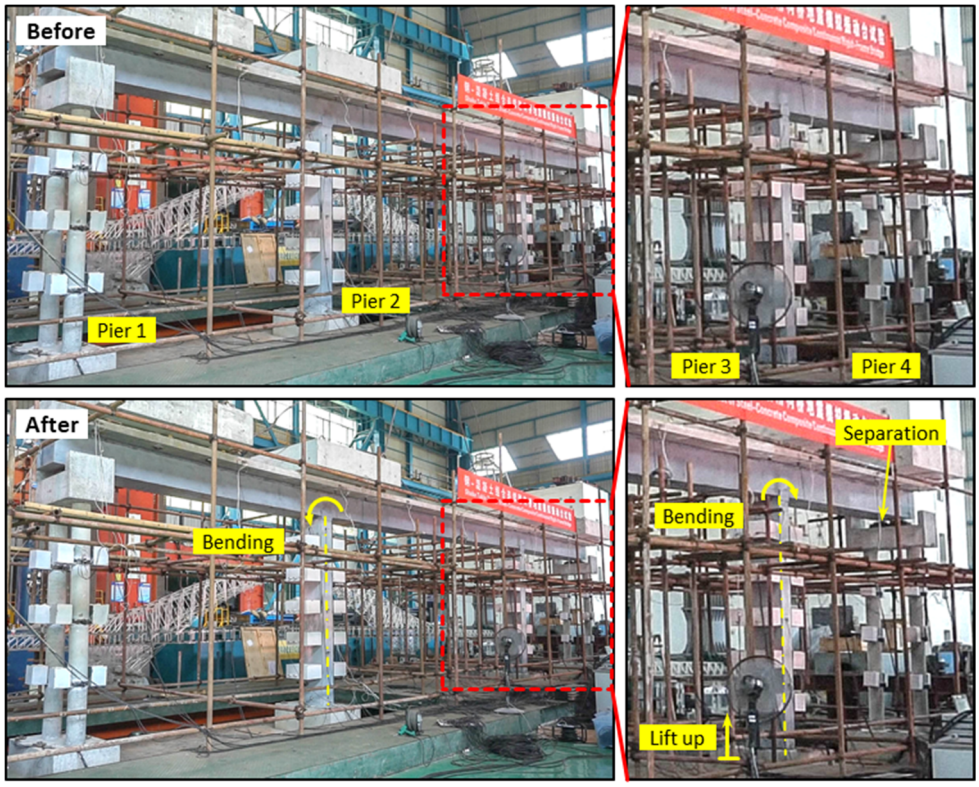

Fig. 4. Recorded deformations of the bridge model in Case 4.

Fig. 5. Damages occurred to the middle piers: (a-b) local buckling of the steel skins; (c-d) crushing of the infilled concrete.

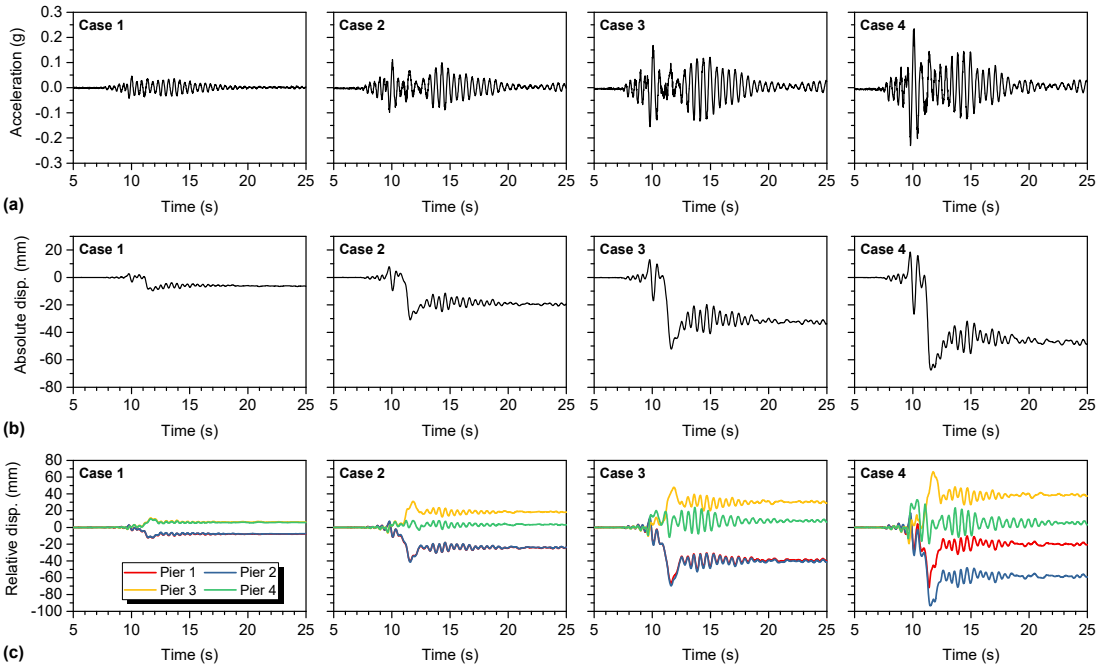

Fig. 6. Bridge responses to the across-fault ground motions in the longitudinal direction: (a) acceleration and (b) absolute displacement time histories of bridge girder; (c) relative displacement time histories of bridge piers.

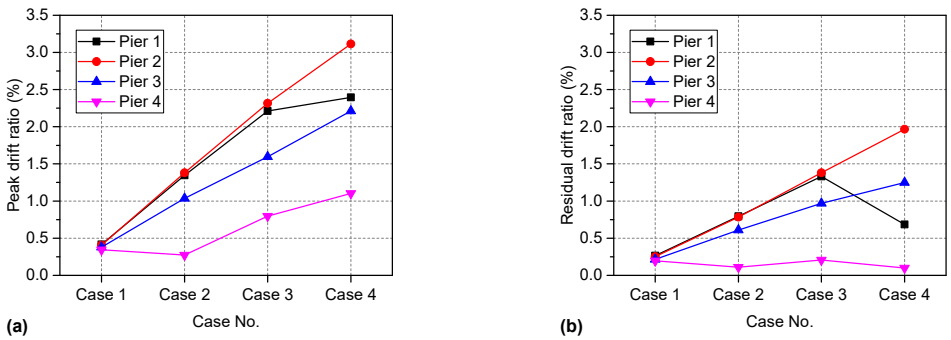

Fig. 7. Longitudinal drift ratios of the four bridge piers: (a) peak; (b) residual.

5. CONCLUSIONS

In this study, shake table tests were performed to investigate the seismic performance of SCCRFB with CFDST piers subjected to crossing-thrust fault ground movements. Testing results show that the damages mainly occurred at the upper and lower ends of the two middle piers with yielding and local buckling of the steel skins and cracks and crushing of the infilled concrete. However, these damages were relatively local and minor, and the whole bridge behaved robustly. The structural responses indicated that the quasi-static components dominated the bridge responses while the dynamic components were relatively small. All the test results verified that the SCCRFB with CFDST piers has very good seismic resistance capabilities and is a potential solution for constructing bridges near or above an active fault.

ACKNOWLEDGEMENTS

This study was supported by the National Key Research and Development Program of China (No. 2017YFC0703405). The first author also appreciates the financial support provided by the Postgraduate Research & Practice Innovation Program of Jiangsu Province (No. KYCX17_0128), the Fundamental Research Funds for the Central Universities, and the China Scholarship Council.

REFERENCES

Goel, R. K. and A. K. Chopra (2009) Linear analysis of ordinary bridges crossing fault-rupture zones, Journal of Bridge Engineering, ASCE Vol 14, pp 203-215.
Goel, R. K. and A. K. Chopra (2009) Nonlinear analysis of ordinary bridges crossing fault-rupture zones, Journal of Bridge Engineering, ASCE Vol 14, pp 216-224.
Kawashima, K. (2002) Damage of bridges resulting from fault rupture in the 1999 Kocaeli and Duzce, Turkey earthquakes and the 1999 Chi-Chi, Taiwan earthquake, Structural Engineering/Earthquake Engineering Vol 19, pp 179s-197s.
Lin, Y., Z. Zong, S. Tian, et al. (2018) A new baseline correction method for near-fault strong-motion records based on the target final displacement, Soil Dynamics and Earthquake Engineering Vol 114, pp 27-37.
Roussis, P. C., M. C. Constantinou, M. Erdik, et al. (2003) Assessment of performance of seismic isolation system of Bolu Viaduct, Journal of Bridge Engineering, ASCE Vol 8, pp 182-190.
Saiidi, M. S., A. Vosooghi, H. Choi, et al. (2013) Shake table studies and analysis of a two-span RC bridge model subjected to a fault rupture, Journal of Bridge Engineering, ASCE Vol 19, pp A4014003.
Shin, T.-C. and T.-l. Teng (2001) An overview of the 1999 Chi-Chi, Taiwan, earthquake, Bulletin of the Seismological Society of America Vol 91, pp 895-913.
Somerville, P. G. (2002) Characterizing near fault ground motion for the design and evaluation of bridges, Third National Seismic Conference and Workshop on Bridges and Highways, Portland, Oregon,
Ucak, A., G. P. Mavroeidis and P. Tsopelas (2014) Behavior of a seismically isolated bridge crossing a fault rupture zone, Soil Dynamics and Earthquake Engineering Vol 57, pp 164-178.
Xu, L. and M. Lin (2017) Analysis of buried pipelines subjected to reverse fault motion using the vector form intrinsic finite element method, Soil Dynamics and Earthquake Engineering Vol 93, pp 61-83.
Yang, S. and G. P. Mavroeidis (2018) Bridges crossing fault rupture zones: A review, Soil Dynamics and Earthquake Engineering Vol 113, pp 545-571.